Photo-assisted ALD: Process Development and Application Perspectives

Ville Miikkulainen[a], Katja Väyrynen[a], Väinö Kilpi[b], Zhongmei Han[a], Marko Vehkamäki[a], Kenichiro Mizohata[c], Jyrki Räisänen[c], and Mikko Ritala[a]
[a] Department of Chemistry, University of Helsinki, A.I. Virtasen aukio 1, FI-00560, Finland
[b] Picosun Oy, Masalantie 365, FI-02430 Masala, Finland
[c] Department of Physics, University of Helsinki, Pietari Kalmin katu 2, FI-00560, Finland

Atomic layer deposition (ALD) is a highly versatile thin-film deposition method that is presently utilized in many steps within microelectronic process flow and is gaining more and more interest in other fields of industry as well. The prosperity of ALD originates from its capability to controllably deposit high-quality films uniformly and conformally over large areas and complicated features. However, one of the main challenges of ALD, lateral control of film growth, stems from these same properties. Selective-area ALD (S-ALD) is presently a subject of intense research and development work as the targeted feature sizes in the semiconductor applications have reduced to a level exceeding the capabilities of lithography methods. Photo-assisted ALD (Photo-ALD) is a less-studied approach to facilitate S-ALD and selection of materials accessible with Photo-ALD is scarce. The present paper contributes to this field by reporting studies on Photo-ALD processes for metal oxides and metals.

Introduction

Atomic layer deposition (ALD) is a thin film deposition technique related to chemical vapor deposition. ALD is based on alternately repeated, saturative and irreversible gas-solid reactions. Typically two gaseous compounds are employed as precursors. The ALD sequence proceeds in a step-by-step, cyclic manner that enables accurate control over the film thickness by adjusting the number of deposition cycles (1). Self-limiting, saturative reactions make ALD films extremely conformal even on complex-shaped nanostructures and large area substrates.

The inherent property of ALD to deposit the films uniformly over complex and large-area substrates turns into a challenge if the film deposition is desired only on selected areas. This applies for example for microelectronics applications, where high-resolution patterning is required. One approach to selective-area ALD (S-ALD) is to deposit passivation layers onto selected parts of the substrate surface prior to ALD so that the film does not grow on those areas (2,3). Self-assembled monolayers (SAMs) and polymers are typically employed for this purpose. Oxides nucleate readily on most surfaces, however, and especially SAMs suffer from degradation when the S-ALD is continued further. In addition, activation layers can be deposited onto the designated parts of the surface on which the ALD film then solely grows. This is mostly applicable for metal films only which have much higher nucleation preference on metallic surfaces than others (4,5). With the activation approach for S-ALD, no removal or etching of the SAMs

or polymers are required. This results in fewer processing steps in the manufacturing flow. The most advanced approach for S-ALD is to employ inherently selective ALD chemistry, so that the film grows solely on the desired substrate material(s). With this approach also the activation step can be omitted. The selection of inherently selective ALD processes is mainly limited to metals for the same reason as with the activation approach (6).

One, less-studied approach to S-ALD is photo-assisted ALD (Photo-ALD). In Photo-ALD, photons at ultraviolet (UV) or visible range are employed to supply energy to the surface reactions. The additional energy provided by the photons potentially allows lower deposition temperatures compared to thermal processes and modifies properties of the film. S-ALD can be realized by simply shadowing the areas where deposition is not wanted but this allows only modest resolution in patterning. For the highest resolution, as needed in state of the art microelectronics, the photoactivation needs to couple with the underlying materials so that the photons activate the growth only on the desired materials on the surface, i.e. through inherently selective ALD. There are only limited number of papers reporting photo-ALD processes, apparently mostly due to challenging construction of the photo-ALD reactors. The studied materials include GaAs, ZnO, Ta_2O_5, ZrO_2, BN, TiO_2 and Al_2O_3 (7-19).

Alkoxides have been used as Photo-ALD precursors for depositing metal oxides. In a paper by Lee et al. tantalum ethoxide was used as metal precursor (14). Utilizing UV lamp with 185-nm emission, they employed two different process schemes for the Photo-ALD process. The single-source approach $Ta(OEt)_5$-purge-irradiation resulted in a growth rate of 0.26 Å per cycle which increased to 0.37 Å per cycle when O_2 was used as a reactant during the irradiation. For both approaches, the growth rate was fairly constant within the process temperature window between 200-300 ºC. Another group has demonstrated Photo-ALD of ZrO_2 at a low deposition temperature of 20 ºC from zirconium tert-butoxide combined with water and simultaneous UV exposure (Xe lamp with main emission peak at 254 nm) (17). However, this approach can be considered as photo-enhanced process as the metal precursor and water deposit ZrO_2 also without UV, even though at higher temperatures. Recently, Chalker et al. reported Photo-ALD of Al_2O_3 and TiO_2 (19). In their approach, UV-excited (main UV emission peaks at 125 nm and 160 nm) O_2 was used as co-reactant at low deposition temperature of 60 ºC. S-ALD was facilitated by masking, but the feature resolution was limited due to diffusion of photo-excited oxygen on the masked area. No Photo-ALD processes for metals have been reported to our knowledge. Our aim is to contribute especially to this unexplored field and develop novel Photo-ALD metal processes for various applications.

Recently, an ALD process approach of the same type as Photo-ALD has been demonstrated by Henke et al. where high-intensity, pulsed visible-infrared light is employed to facilitate flash-enhanced ALD (FEALD) (20). The essential difference of F-ALD from Photo-ALD is that the light is utilized to deliver short pulses of heat on the surface and thereby drive the surface reactions, whereas in Photo-ALD photolysis is the desired mechanism for facilitating reduced deposition temperatures and S-ALD. FEALD has been reported to deposit Si, Ru, and Al_2O_3 (20,21).

Experimental

Film Deposition

Films were deposited on full 150-mm Si (100) wafers or pieces cut from the wafers if not stated otherwise. Picosun™ R-200 reactor specially modified for Photo-ALD was used for the depositions. Two alternative UV sources were employed. First option is an RC-800 series pulsed xenon discharge light source from Xenon Corporation. The lamp produces high-intensity pulsed light with a broad wavelength spectrum from 190 to 800 nm. The optical window between the reactor and the light source was made of fused silica (Finnish Specialglass) transmitting light down to 190 nm in wavelength. The window was purged with N_2 to prevent film deposition on it. No gate valve or other physical shutter is needed since the pulsing of light can be controlled and synchronized through the ALD reactor software. Second option was a deuterium lamp from Hamamatsu (Model L11798) producing photons in the range between 115 and 400 nm. A MgF_2 optical window integrated into the VUV source secured high UV transmission within the emission range. With this option, a gate valve was used to control the illumination at the desired ALD cycle phase and Ar curtain flow protected the optical window from film deposition. Control of both the light sources is fully integrated into the ALD reactor software. Substrate holder temperature was monitored with a thermocouple.

Metal precursors were titanium isopropoxide ($Ti(O^iPr)_4$), zirconium tert-butoxide ($Zr(O^tBu)_4$), hafnium tert-butoxide ($Hf(O^tBu)_4$), niobium ethoxide ($Nb(OEt)_5$), tantalum ethoxide ($Ta(OEt)_5$), cyclohexadiene tricarbonyl ruthenium ($Ru(chd)(CO)_3$), copper bis(dimethylaminopropoxide) ($Cu(dmap)_2$), and (2,2-dimethyl-6,6,7,7,8,8-heptafluoro-octane-3,5-dionato) silver(I) triethylphosphine ($Ag(fod)PEt_3$) and they were evaporated from PicoHot™ source. Vanadyl isopropoxide ($VO(O^iPr)_3$) was also tested as a Photo-ALD precursor for vanadium oxide but no controllable growth conditions were found.

Film Characterization

Film crystallinity and crystal phases were characterized by X-ray diffraction (XRD, Panalytical X'Pert Pro) with parallel beam optics and grazing incidence measurement geometry (incidence angle 1.0 °). Scanning electron microscopy (SEM, Hitachi S-4800) and transmission electron microscopy (TEM) were used for analyzing film morphology and, from the cross-sections, film conformality. Film thicknesses were determined by UV-VIS reflectometry or X-ray reflection (XRR) when the film thickness was too low for reliable analysis by UV-VIS. XRR was also used for analyzing the densities of the deposited films. Time-of-flight elastic recoil detection analysis (ToF-ERDA) was used to characterize the composition of the films, including their elemental depth profiles. Dielectric properties of the oxide films were characterized by current-voltage (I-V) and capacitance-voltage (C-V) methods.

Results and Discussion

Metal Oxide Depositions from Metal Alkoxides with Single-source Approach

For TiO_2, ZrO_2, HfO_2, Nb_2O_5, and Ta_2O_5, Photo-ALD process was realized with the single-source approach, i.e. without any additional oxygen source or other reactant besides the metal alkoxide that thus served as both metal and oxygen source. The process

sequence was alkoxide pulse – 5 s purge – UV exposure with Xenon lamp. For Ta_2O_5, the process characteristics were systematically studied. First, the saturation with respect to UV exposure was demonstrated, as illustrated in Figure 1. Growth rate saturates at 0.12 Å/cycle with 30 flashes. The growth rate is lower than reported by Lee et al. for the same precursor system, probably due to different UV emission employed (14). It is also lower than the growth rate in the corresponding thermal ALD process with water as the oxygen source (22). This can be explained by larger steric hindrance between $Ta(OEt)_5$ adsorbates in Photo-ALD whereas in the thermal process some of the ligands may be released in reactions with hydroxyl groups already during the $Ta(OEt)_5$ pulse.

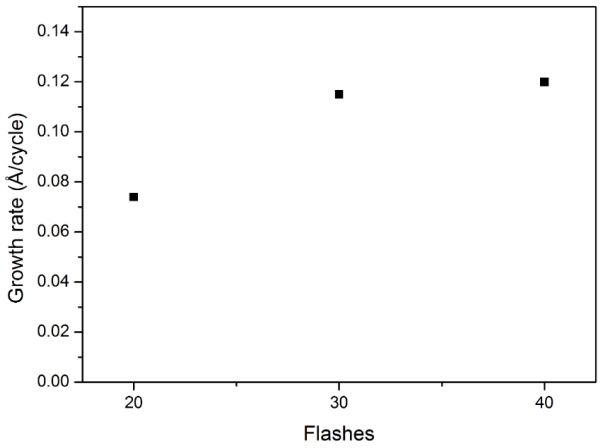

Figure 1. Photo-ALD Ta_2O_5 growth rate as a function of UV flashes (5 Hz flash frequency) at deposition temperature of 245 ºC.

Growth rate as a function of deposition temperature was studied for accessing the feasible temperature range for the process. At 200 ºC, the growth rate was 0.075 Å/cycle, and at 150 ºC 0.035 Å/cycle. The feasibility for S-ALD was studied by employing a set of two aluminum shadow masks resulting in a University of Helsinki emblem on a 150-mm Si wafer (Figure 2). It should be noted that the spatial resolution of the features does not allow semiconductor device-level patterning but could be used for example for protecting contact areas or blocking growth on the wafer backside.

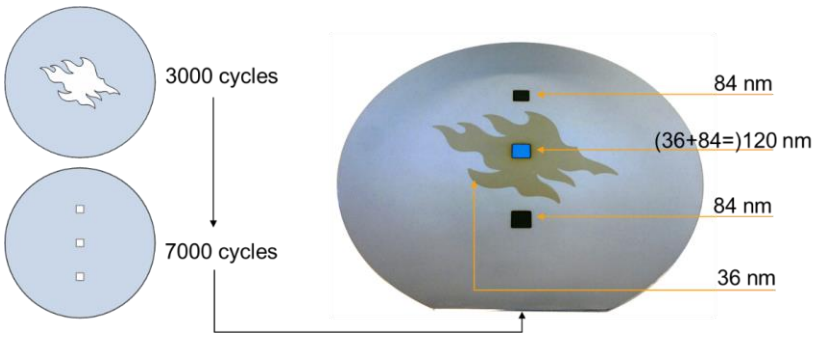

Figure 2. Demonstration of area-selective deposition by Photo-ALD Ta_2O_5 employing set of aluminum shadow masks (0.3 mm wafer-substrate distance) at deposition temperature of 245 ºC, with 30 UV flashes/cycle.

To get insight into the fundamentals of the photo-assisted surface process, a simple optical filtering was done to cut off spectral ranges that reach the substrate surface. Slides of soda lime and borosilicate glasses were placed above the substrate (slide to substrate distance approximately 0.5 mm) to block UV with wavelengths shorter than around 300 and 350 nm. It was found that both glass slides blocked the film growth. This finding leads into two conclusions. First, the effective band of the lamp emission spectrum for the surface process is obviously 190-300 nm. Second, as most of the emission spectrum (300-800 nm) is transmitted through the filtering glass slides and thereby most of the overall photon flux reaches the substrate, it appears that the photo-process is more likely driven by electronic transitions rather than surface heating as a result of intensive illumination. Moreover, to get insight into the photo-process, we studied the Photo-ALD growth on patterned substrate. In Figure 3, SEM cross-section on Ta_2O_5 deposited on Si pillars shows that on surfaces at the bottom of the pillar structure, perpendicular to the direction of the incoming light, the film is of the same thickness as measured on flat silicon. However, on surfaces parallel to the incoming light the film is notably thinner. If the Photo-ALD process was driven by heat generated by the intensive light, it would be expected that the film thickness is almost the same on the pillar walls since heat would easily transfer from the tip through the pillar. Henke et al. discussed this type of behavior for patterned silicon in their FEALD setup where visible and infrared light is employed for rapid heating of the surface (20). In FEALD, the temperature of the Si substrate is expected to be uniform down to 6 μm and thereby the film thickness on surfaces parallel to light should be uniform within that range (20,21). Our findings can be concluded to support photolytic mechanism for our Photo-ALD Ta_2O_5 process.

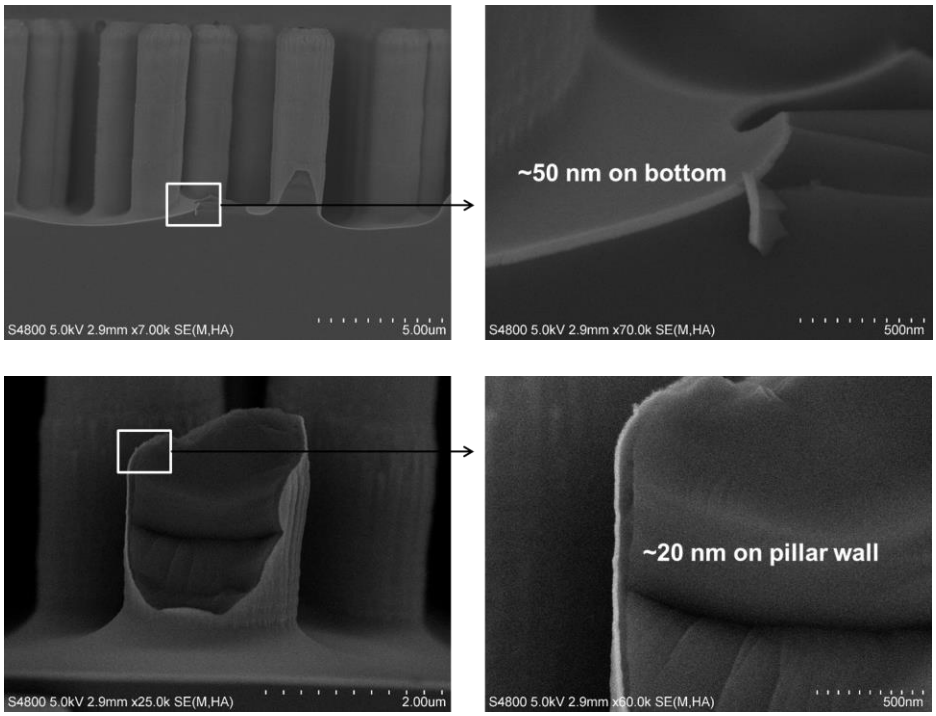

Figure 3. Cross-section SEM on pillar-structured Si with Photo-ALD Ta_2O_5: overview (left-top), magnification of the bottom of the structure (right-top), broken pillar (left-bottom), magnification of pillar wall (right-bottom). The UV direction during Photo-ALD was from the top to the bottom of the structure.

In addition to Ta_2O_5, films of TiO_2, ZrO_2, HfO_2 and Nb_2O_5 can be deposited by Photo-ALD from the corresponding metal alkoxides. These processes were less systematically studied aiming just to demonstrate the versatility of the alkoxide single-source approach. For TiO_2, deposited from $Ti(O^iPr)_4$, the growth rate varied between 0.07 and 0.12 Å per cycle as the deposition temperature varied between 200 and 245 ºC. Analogously to Ta_2O_5, optical filtering with soda lime and borosilicate glasses resulted in blocking the film growth suggesting that similar wavelength ranges are responsible for the film growth chemistries in the two processes, and that photolytic mechanism prevails in the case of TiO_2 Photo-ALD as well. ZrO_2 and HfO_2, deposited from their tetra-tert-butoxides, showed similar growth properties: their growth rates varied from around 0.07 to around 0.3 Å per cycle, deposited with 30 UV flashes at temperatures of 150 and 245 ºC, respectively. At 245 ºC, HfO_2 growth was observed under a shadow mask indicating minor thermal decomposition of the precursor at that deposition temperature. Growth rate of Nb_2O_5, deposited from $Nb(OEt)_5$, varied between 0.03 and 0.09 Å per cycle as the deposition temperature varied between 180 and 245 ºC, respectively.

Photo-ALD Nb_2O_5 and Ta_2O_5 films were amorphous whereas TiO_2, ZrO_2, and HfO_2 showed crystalline features in XRD. TiO_2 films were weakly crystalline in the rutile phase that is different from the thermal ALD TiO_2 which typically adopts the anatase phase when deposited at these temperatures on Si (1). Phase content of Photo-ALD ZrO_2 films was a mixture of the cubic and monoclinic phases. The diffraction peaks had relatively high FWHM values suggesting nanocrystalline structure. For HfO_2, only the monoclinic phase was visible and the morphology was nanocrystalline as the diffraction peaks were broad like for ZrO_2.

TABLE I. ToF-ERDA elemental compositions in atomic percentage for Photo-ALD oxide films, deposition temperatures included.

Element	**TiO_2 225 ºC**	**ZrO_2 150 ºC**	**HfO_2 150 ºC**	**Nb_2O_5 250 ºC**	**Ta_2O_5 250 ºC**
M	34.3	29.5	28.6	28.4	25.0
O	64.7	61.3	66.8	67.3	66.4
C	0.08	2.6	1.6	1.2	1.4
H	0.9	6.3	2.7	3.2	7.2
F	-	0.32	0.3	-	-
Cl	0.07	-	-	-	-
stoich.	$TiO_{1.9}$	$ZrO_{2.1}$	$HfO_{2.3}$	$Nb_2O_{4.7}$	$Ta_2O_{5.3}$

As demonstrated by the ToF-ERDA results in Table I, Photo-ALD oxides were relatively pure from impurities considering that no oxidant was used for the depositions. Minor fluorine and chlorine impurities originate most likely from the precursors. Regarding stoichiometry, TiO_2 and more notably Nb_2O_5 showed some oxygen deficiency whereas all the other studied oxides were stoichiometric or slightly oxygen rich. XRR study on Nb_2O_5 showed increasing density from 4.75 to 5.1 g/cm^3 as a function of deposition temperature from 180 to 245 ºC. These density values lie between the crystallographic densities of 4.55 and 5.24 for the monoclinic and orthorhombic Nb_2O_5 phases, respectively. The oxygen deficiency and high density of the films suggest that Nb may be partially reduced from the original +V in the ethoxide to +IV upon the Photo-ALD process. Investigation with photoelectron spectroscopy or X-ray absorption spectroscopy would be required to draw decisive conclusions on the oxidation states of the metals.

In a preliminary study to characterize the dielectric properties of the HfO_2 films, metal-insulator-metal capacitor structure was made with continuous platinum bottom electrode deposited on silicon by electron beam evaporation (EBE), 50-nm HfO_2 as insulator layer by Photo-ALD, and patterned aluminum as top electrode by EBE through a shadow mask. The top electrode area per capacitor was $2.04 \cdot 10^{-7}$ m^2. After brief ageing with 5-V bias over the film, stable capacitance of 420 pF was achieved at 10 kHz frequency with a dielectric loss of 0.022. Calculated dielectric constant was 11.6.

Metal Depositions

Deposition Experiments with Deuterium Lamp. To complement the emission wavelength range provided by the xenon lamp, Photo-ALD reactor was adapted to house a Hamamatsu deuterium VUV lamp. Ruthenium was deposited using the deuterium lamp from $Ru(chd)(CO)_3$ on various substrates. It was found that the deposition was selective to the substrate material and film did deposit on Si, ALD-Al_2O_3, ALD-TiO_2, and ALD-Ta_2O_5, but not on ALD-TiN. However, deposition of ALD-Al_2O_3 on TiN initiated the Ru film growth, if more than 50 trimethyl aluminum-water cycles were applied. It was also noted that the achievable film thickness by Photo-ALD Ru is limited: as the film becomes uniform and reaches a certain thickness, the film growth appears to terminate to a thickness of around 35 nm. Even extensive number of Photo-ALD cycles did not deposit thicker Ru films. SEM micrograph of a 34-nm Ru film (Figure 4) demonstrates the small grain size of the material and compositional analysis by ToF-ERDA gives elemental constitution of 76 at.-% Ru; 6.6 at.-% O; 14 at.-% C; 3.6 at.-% H. These findings suggest that the photochemistry actually takes place in the substrate and as the substrate becomes covered by a thick enough Ru film, an optically absorbing material, the photons no more reach the substrate to enable the Photo-ALD process. Furthermore, the relatively high impurity content testifies for incomplete surface reactions or parasitic reactions driven by the catalytic nature of the Ru surface. Photo-ALD experiments where oxygen gas was added during the UV period for enhancing the surface reactions did not improve the film quality.

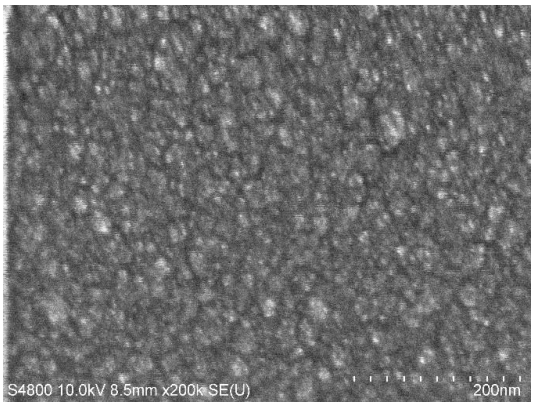

Figure 4. SEM micrograph on 34-nm Photo-ALD Ru film on Si, deposited at 125 ºC.

Deposition Experiments with Xenon Lamp. Copper was deposited by Photo-ALD from $Cu(dmap)_2$ with xenon lamp. Analogously to the Ru case above, the growth process was substrate selective. In this case, the selectivity was even more prominent. ALD-Ta_2O_5 was found to provide the most favorable starting surface, where copper-colored,

uniform films deposited with a distinct shadow area from the mask. However, also analogous to the Ru case, the Photo-ALD Cu process appeared to deposit films up to a limited thickness of around 60 nm, and even extensive number of Photo-ALD cycles did not increase the film thickness The Cu grains coalesce upon increasing the Photo-ALD cycle count, as illustrated by the SEM micrographs in Figure 5. As with the Ru case, it appears that the photolytic deposition process is driven by the substrate. The Cu films deposited with 4000 and 5000 cycles were conductive for which sheet resistances of 1.41 and 0.94 Ω/□, respectively, were measured. Thereby resistivity for the 5000-cycle, 60-nm Cu film is 5.7 μΩ·cm, which is in good comparison to bulk Cu resistivity of 1.7 μΩ·cm considering that the film has narrow gaps in between the continuous matrix (Figure 5).

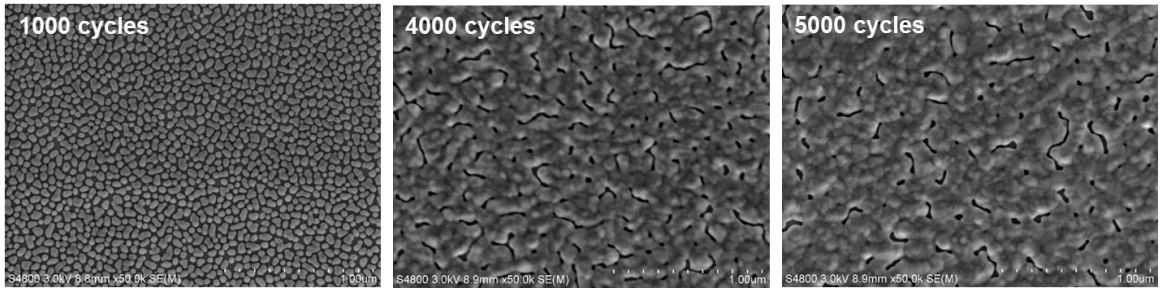

Figure 5. SEM micrographs on Photo-ALD Cu film on ALD-Ta_2O_5, deposited at 150 ºC with different number of ($Cu(dmap)_2$ – UV (6 flashes)) cycles.

On polycrystalline anatase ALD-TiO_2, the Cu Photo-ALD process exhibited interesting growth properties. By SEM, Cu deposits were found on defined areas whereas other areas were almost free from Cu deposits (Figure 6). Areas rich in Cu deposits seem to follow grain boundaries of the underlying TiO_2 film, and the Cu aggregates have high preference over some of the TiO_2 grains. To get more insight into this behavior, cross-section TEM study was conducted.

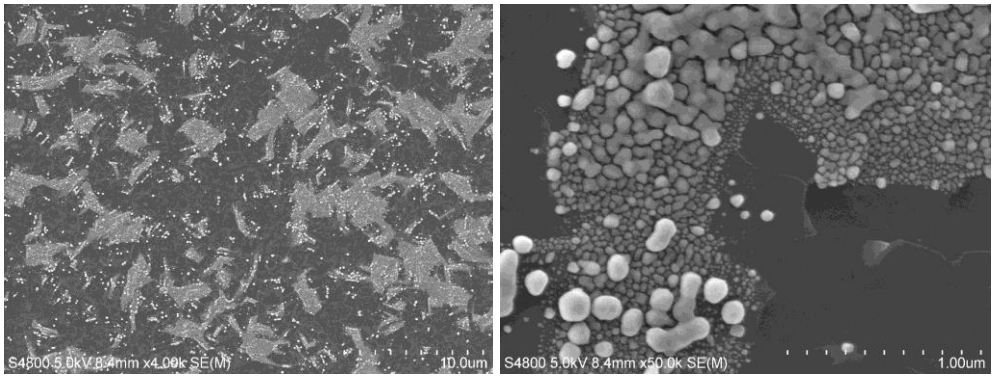

Figure 6. SEM micrographs on Photo-ALD Cu, deposited at 150 ºC on ALD-TiO_2 film: overview (left) and magnification on a defined area (right).

In TEM, even more atypical morphology was found: the Cu deposit seems to have grown even under one of the TiO_2 grains that have partially lifted off from the substrate (Figure 7). This behavior can be hypothesized to originate from two optional mechanisms. The first option is that the Cu Photo-ALD is highly selective over substrate and the UV

light is intensive enough to transmit through the TiO_2 grain to facilitate Cu Photo-ALD also under the TiO_2 grain, provided that the TiO_2 grain was released from the underlying Si substrate before the Cu Photo-ALD. The second option is that the Cu Photo-ALD is isotropic regarding the anatase grain orientation but after initial photolytic reaction that releases the ligands, Cu is mobile and grains coalesce via Ostwald ripening mechanism. The overall mechanism can be also a combination of these considering the long distances between the preferred Cu deposition areas and the grain size distribution over a TiO_2 grain: Cu grains are larger in the center of the TiO_2 grain suggesting surface Cu diffusion process over a single TiO_2 grain.

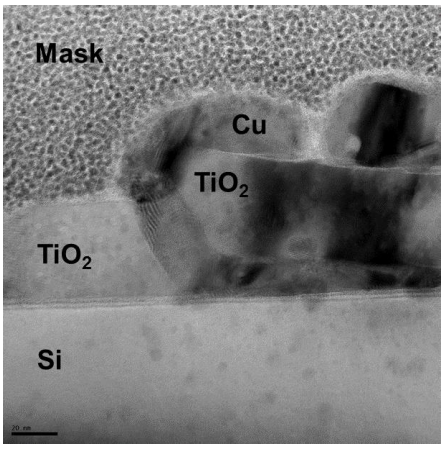

Figure 7. Cross-section TEM on Photo-ALD Cu on ALD-TiO_2 scale bar 20 nm.

The obviously highly selective nature of the Photo-ALD Cu process can be exploited for inherently selective deposition on Ta_2O_5 only, without masking nor passivation layers. Demonstration of such selective deposition is illustrated in Figure 8, where Cu is deposited by Photo-ALD on a cross-section of an ALD laminate of Al_2O_3 (100 nm)| Ta_2O_5 (60 nm) | Al_2O_3 (100 nm) | Ta_2O_5 (20 nm) | Al_2O_3 (100 nm). The selectivity is remarkably high considering the narrow width of the features and gives promise for the scale required for device-level patterning, yet the material combinations and continuity of the Photo-ALD Cu remain to be studied further.

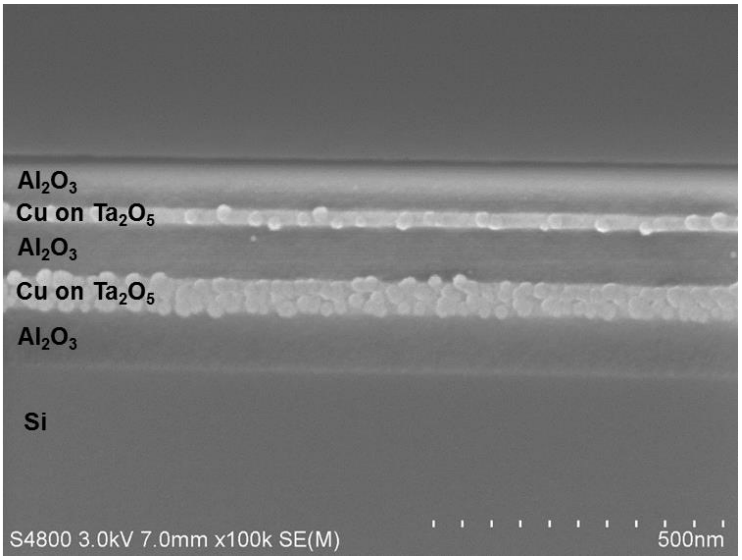

Figure 8. Photo-ALD Cu on cross-section of ALD Al_2O_3-Ta_2O_5 laminate demonstrating high selectivity of Cu on Ta_2O_5 over both Al_2O_3 and Si.

Metal Photo-ALD of Ni and Ag showed very similar behavior as observed with Cu. For Ni deposited from $Ni(dmap)_2$ at 150 ºC, selectivity was observed on Ta_2O_5 and TiO_2 over Si and Al_2O_3. On Ta_2O_5 and TiO_2, as illustrated by SEM in Figure 9, the film deposits as small grains uniformly over the substrate whereas on Si and Al_2O_3 the nuclei density was notably lower (not shown).

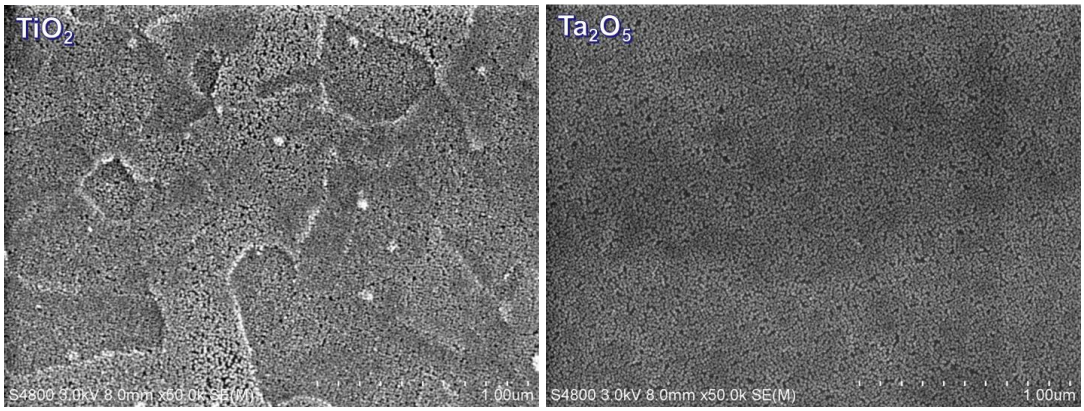

Figure 9. SEM micrographs of Photo-ALD Ni deposited from $Ni(dmap)_2$ on TiO_2 and Ta_2O_5 films.

In line with the observations on the other metals, Photo-ALD Ag from $Ag(fod)PEt_3$ showed surface-selective deposition characteristics. Good nucleation was observed on Si, ALD-Al_2O_3, and soda lime glass, with morphology similar to those found for the other metals. On ALD-Ru and ALD-TiN the Ag nucleation was poor. On ALD-TiO_2, the nucleation seems to be uniform as Ag dots are spread over the substrate, but in addition to that, Ag dendrites are observed (Figure 10). Some of the dendrites are originating underneath the TiO_2 grains suggesting similar mechanism as hypothesized for Cu Photo-ALD. The Ag dendrites seem to have lifted some of the TiO_2 grains off from the substrate during the Ag Photo-ALD, similarly to the Cu case. If such a particle size and dispersion could be controlled by Photo-ALD process variables, this approach could be potentially applied for catalytic and plasmonic applications.

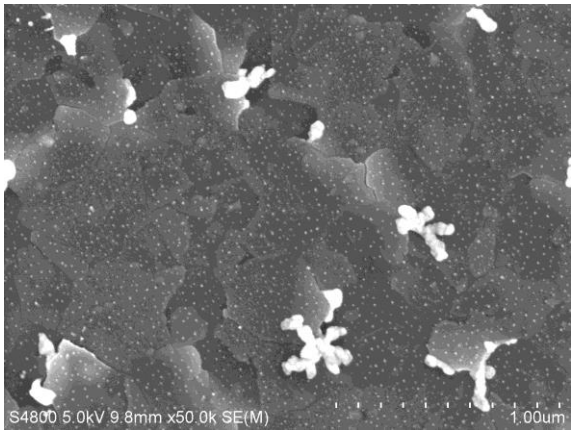

Figure 10. Photo-ALD Ag on anatase ALD-TiO_2. White Ag dots are uniformly spread over the surface. In addition, there are some scattered larger Ag dendrites, some of which originate underneath the ALD-TiO_2 grains.

Conclusions

In the present paper, we have reported Photo-ALD studies on several oxide materials and metals utilizing a customized Picosun™ ALD reactor with two alternative UV sources. Metal oxides can be deposited in a controlled manner from their metal alkoxides employing the single-source approach, i.e. with the alkoxide-purge-UV sequence. This approach allows S-ALD using shadow masks. The oxides are pure and stoichiometric, except for the case of Nb_2O_5, where oxygen deficiency was evident from the compositional analysis.

Metal Photo-ALD, as studied with several processes and metals, turned out to be complicated and substrate proved to play an essential role in the photolytic process. The high surface selectivity of the metal processes could be potentially utilized even in the device-level patterning provided that material combinations and morphology of the deposited metal can be better controlled. Moreover, high mobility of the deposited metals leads into analogous and interesting morphologies that need to be studied in more detail to understand the fundamental mechanisms behind the processes. Nevertheless, the preliminary results presented here provide an encouraging, novel pathway to deposit metal films and nanoparticles by Photo-ALD.

Acknowledgments

Semiconductor Research Corporation (SRC) and Finnish Centre of Excellence in Atomic Layer Deposition (ALDCoE) are gratefully acknowledged for funding this research. Picosun provided the specially modified Photo-ALD reactor for this project. Dr. Marianna Kemell is acknowledged for help in acquiring the SEM images.

References

1. V. Miikkulainen, M. Leskelä, M. Ritala and R. L. Puurunen, *J. Appl. Phys.*, **113**, 021301 (2013).
2. X. Jiang and S. F. Bent, *J. Phys. Chem. C*, **113**, 17613 (2009).
3. E. Färm, M. Kemell, M. Ritala and M. Leskelä, *Chem. Vap. Deposition*, **12**, 415 (2006).
4. E. Färm, S. Lindroos, M. Ritala and M. Leskelä, *Chem. Mater.*, **24**, 275 (2012).
5. A. J. M. Mackus, A. A. Bol and W. M. M. Kessels, *Nanoscale*, **6**, 10941, (2014).
6. B. Kalanyan, P. C. Lemaire, S. E. Anatasov, M. J. Ritz and G. N. Parsons, *Chem. Mater.*, **28**, 117 (2016).
7. A. Doi, Y. Aoyagi and S. Namba, *Appl. Phys. Lett.*, **49**, 785 (1986).
8. Y. Aoyagi, A. Doi, T. Meguro, S. Iwai, K. Nagata and S. Nonoyama, *Chemtronics*, **4**, 117 (1989).
9. Y. Aoyagi, T. Meguro, S. Iwai and A. Doi, *Mater. Sci. Eng., B*, **10**, 121 (1991).
10. Q. Chen and P. D. Dapkus, *Thin Solid Films*, **225**, 115 (1993).
11. A. Yamada, B. Sang and M. Konagai, M., *Appl. Surf. Sci.*, **112**, 216 (1997).
12. K. Saito, Y. Watanabe, K. Takahashi, T. Matsuzawa, B. Sang and M. Konagai, *Sol. Energy Mater. Sol. Cells*, **49**, 187 (1997).

13. Y. Yamamoto, K. Saito, K. Takahashi and M. Konagai, *Sol. Energy Mater. Sol. Cells*, **65**, 125 (2001).
14. Y.-H. Lee, J.-C. Kwak, B.-S. Gang, H.-C. Kim, B.-H. Choi, B.-K. Jeong, S.-H. Park and K.-H. Lee, *J. Electrochem. Soc.*, **151**, C52 (2004).
15. J.-C. Kwak, Y.-H. LeeB.-H. and B.-H. Choi, *Appl. Surf. Sci.*, **230**, 249 (2004).
16. J. Olander, L. M. Ottosson, P. Heszler, J.-O. Carlsson and K. M. E. Larsson, *Chem. Vap. Deposition*, **11**, 330 (2005).
17. B. H. Lee, S. Cho, J. K. Hwang, S. H. Kim and M. M. Sung, *Thin Solid Films*, **518**, 6432 (2010).
18. S. K. Kim, S. Hoffmann-Eifert and R. Waser, *Electrochem. Solid-State Lett.*, **14**, H146 (2011).
19. P. R. Chalker, P. A. Marshall, K. Dawson, I. F. Brunell, C. J. Sutcliffe and R. J. Potter, *AIP Adv.*, **5**, 017115 (2015).
20. T. Henke, M. Knaut, C. Hossbach, M. Geidel, L. Rebohle, M. Albert, W. Skorupa and J. W. Bartha, *ECS J. Solid State Sci. Technol.*, **4**, P277 (2015).
21. T. Henke, M. Knaut, C. Hossbach, M. Geidel, L. Rebohle, M. Albert, W. Skorupa and J. W. Bartha, *ECS Transactions*, **64**, 167 (2014).
22. K. Kukli, M. Ritala and M. Leskelä, *J. Electrochem. Soc.*, **142**, 1670 (1995).